


Conductance oscillations and speed of chiral Majorana mode in a quantum anomalous Hall two-dimensional strip

Javier Osca¹ and Llorenç Serra^{1,2}

¹*Institute of Interdisciplinary Physics and Complex Systems IFISC (CSIC-UIB), E-07122 Palma de Mallorca, Spain*

²*Department of Physics, University of the Balearic Islands, E-07122 Palma de Mallorca, Spain*

 (Received 30 July 2018; revised manuscript received 10 September 2018; published 24 September 2018)

We predict conductance oscillations in a quantum anomalous Hall two-dimensional strip having a superconducting region of length L_x with a chiral Majorana mode. These oscillations require a finite transverse extension of the strip L_y of a few microns or less. Measuring the conductance periodicity with L_x and a fixed bias, or with bias and a fixed L_x , yields the speed of the chiral Majorana mode. The physical mechanism behind the oscillations is the interference between backscattered chiral modes from the second to first interface of the normal-superconductor-normal double junction. The interferometer effect is enhanced by the presence of side barriers.

DOI: [10.1103/PhysRevB.98.121407](https://doi.org/10.1103/PhysRevB.98.121407)

Majorana modes in condensed matter systems are objects of an intense research due to their peculiar exchange statistics that could allow implementing a robust quantum computer [1]. A breakthrough in the field was the observation of zero-bias anomalies in semiconductor nanowires with proximity-induced superconductivity [2]. Although an intense theoretical debate has followed the experiment, evidence is now accumulating [3,4] that these quasi-one-dimensional (1D) systems indeed host localized Majorana states on their two ends, for a proper choice of all the system parameters (see Refs. [5,6] for recent reviews).

Another breakthrough is the recent observation of a peculiar conductance quantization, $0.5e^2/h$, in a quantum anomalous Hall (QAH) two-dimensional (2D) (thin) strip, of 2×1 mm [7]. A region of $L_x \approx 0.8$ mm in the central part of the strip is put in proximity of a superconductor bar, whose influence makes the central piece of the strip become a topological system able to host a single chiral Majorana mode. The device can then be seen as a generic normal-superconductor-normal (NSN) double junction with tunable topological properties. The hallmark of transport by a single chiral Majorana mode in the central part is the observed halved quantized conductance, since a Majorana fermion is half an electron and half a hole [8–13].

The observed signal of a chiral Majorana mode in the macroscopic device of Ref. [7] naturally leads to the question of how is this result affected when the system dimensions are reduced and quantum properties are enhanced. Can the presence of a Majorana mode still be clearly identified in a smaller strip? Are there additional *smoking-gun* signals? In this Rapid Communication we provide theoretical evidence predicting a positive answer to these questions. In a smaller strip, with a lateral extension L_y of a few microns or less, we predict the existence of conductance oscillations as a function of L_x (the longitudinal extension of the superconducting piece) and a fixed longitudinal bias. Alternatively, oscillations are also present as a function of bias and a fixed value of L_x .

We find that the period of the conductance oscillations is related to the speed c of the chiral Majorana mode, as defined from the linear dispersion relation $E = c\hbar k$ with k the mode wave number. More precisely, the oscillating part of the conductance is $\approx \delta G \cos(2L_x E/\hbar c)$. Therefore, measuring the distance ΔL_x between two successive conductance maxima in a fixed bias V (equivalent to a fixed energy E since $E = eV/2$), it is $c = \Delta L_x E/\pi\hbar$. Analogously, in a device with a fixed L_x , the distance ΔE between two successive bias maxima yields $c = L_x \Delta E/\pi\hbar$. As anticipated, this result implies the possibility of a purely electrical measurement of the speed of a chiral Majorana mode and it thus provides an additional hallmark of the presence of such peculiar modes.

A narrow strip (typically $L_y \lesssim 1 \mu\text{m}$) is required for a sizable oscillation amplitude δG , otherwise, it becomes negligible when L_y increases. The amplitude is also weakly dependent on the energy, yielding a slightly damped oscillation with bias. The physical mechanism behind the predicted conductance oscillations is the interference of the two backscattered chiral modes of the NSN double junction. An initially reflected mode from the first interface (NS), assuming left to right incidence, is superposed by the reflection from the second interface (SN) that has traveled backwards a distance L_x . A constructive interference yields an enhanced Andreev reflection that, in turn, yields an enhanced device conductance. Since Majorana mode backscattering between the two interfaces can be seen as a manifestation of the hybridization of the two edge modes of the strip, a finite (small) L_y is required for its manifestation as a sizable effect.

Chiral mode backscattering in the presence of Majorana modes was already considered in Ref. [9], but only between interfaces and leads, not in between interfaces, which only occurs in the quantum limit for smaller L_y . We stress that, as discussed in Ref. [9], we assume a grounded superconductor configuration and that conductance is measured with an applied symmetrical bias on both sides. Very recent works [14,15] have considered biased superconductor configurations, focusing on the dependence of the quasiparticle-reversal

transmissions with the chemical potential. Quasiparticle reversal was also discussed with quantum spin Hall insulators in Ref. [16]. Interferometry with Majorana beam splitters was considered in Refs. [17–19], although a conceptual difference with our work is that beam splitters constrain quasiparticles to follow different trajectories while we consider a single material strip. It is also worth stressing that the suggested interference of this work requires traveling modes with a well-defined k , such as chiral Majorana modes, since the oscillations persist for arbitrary large values of L_x . This is an essential difference with hybridization of Majorana (localized) end states in nanowires, lacking a well-defined k , that has been shown to rapidly vanish as L_x increases [20].

Model and parameter values. We consider a model of a double-layer QAH strip with induced superconductivity in the central region as in Ref. [7]. Using vectors of Pauli matrices for the two-valued variables representing usual spin σ , electron-hole isospin τ , and layer-index pseudospin λ , in a Nambu spinorial representation that groups the field operators in the top (t) and bottom (b) layers, $[(\Psi_{k\uparrow}^t, \Psi_{k\downarrow}^t, \Psi_{-k\downarrow}^{t\dagger}, -\Psi_{-k\uparrow}^{t\dagger}), (\Psi_{k\uparrow}^b, \Psi_{k\downarrow}^b, \Psi_{-k\downarrow}^{b\dagger}, -\Psi_{-k\uparrow}^{b\dagger})]^T$, the Hamiltonian reads

$$\mathcal{H} = [m_0 + m_1(p_x^2 + p_y^2)]\tau_z\lambda_x + \Delta_Z\sigma_z - \frac{\alpha}{\hbar}(p_x\sigma_y - p_y\sigma_x)\tau_z\lambda_z + \Delta_p\tau_x + \Delta_m\tau_x\lambda_z. \quad (1)$$

The physical origin of the different parameters has been discussed in Refs. [7–13]. Let us only emphasize here that the superconductivity parameters $\Delta_{p,m}$ are just the half sum or half difference of the corresponding parameter in each layer, $\Delta_{p,m} \equiv (\Delta_1 \pm \Delta_2)/2$, with $\Delta_{1,2}$ vanishing in the left and right normal regions and taking constant values for $x \in [-L_x/2, L_x/2]$ (see sketch in Fig. 1). The strip confinement along the lateral coordinate (y) is obtained by assuming that m_0 takes a large value for $y \notin [-L_y/2, L_y/2]$, effectively forcing the wave functions to vanish at the lateral edges.

It is important to consider realistic values for the Hamiltonian parameters. In our calculations we assume a unit system set by 1 meV as the energy unit, 1 μm as the length unit, and a mass unit m_U from the condition $\hbar \equiv m_U^{1/2}$ meV $^{1/2}$ μm , yielding $m_U = 7.6 \times 10^{-5}m_e$, where m_e is the bare electron mass. We have assumed $\alpha = 0.26$ meV μm , $m_0 = 1$ meV, $m_1 = 10^{-3}m_U^{-1}$, $\Delta_1 = 1$ meV, and $\Delta_2 = 0.1$ meV. The parameter Δ_Z models an intrinsic magnetization of the material and is varied to explore different phase regions, usually with $\Delta_Z < 2$ meV. We take these values as reasonable estimates for QAH insulators based on Cr-doped and V-doped (Bi, Sb) $_2$ Se $_3$ or (Bi, Sb) $_2$ Te $_3$ magnetic thin films [11,12]. Nevertheless, the results we discuss below are not sensitive to small variations around these estimates.

Method. Our analysis is based on the numerical solution of the Bogoliubov–de Gennes scattering equation $\mathcal{H}\Psi = E\Psi$ for a given energy E , assuming an expansion of the wave function in the complex band structure for each portion of the strip where the parameters are constant. An *effective* matching in 2D at the two interfaces of the NSN double junction yields all the scattering coefficients. The method is explained in more detail in the Supplemental Material [21] and is based on Refs. [22–29]. In particular, the conductance for a given

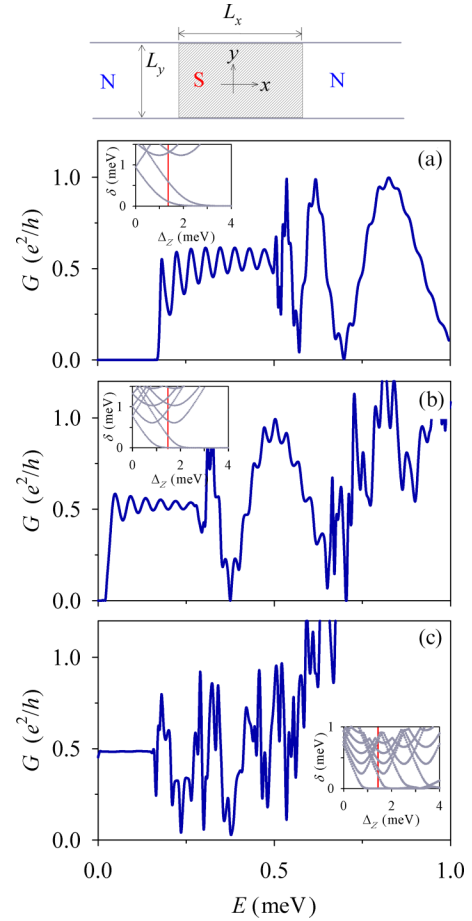


FIG. 1. Upper: Sketch of the physical system. (a)–(c) Conductance as a function of the energy (bias) for (a) $L_y = 1 \mu\text{m}$, (b) $2 \mu\text{m}$, and (c) $5 \mu\text{m}$. The three panels are for $L_x = 20 \mu\text{m}$ and $\Delta_Z = 1.5$ meV. The insets in each panel show the $\delta - \Delta_Z$ phase diagram, with δ the $k = 0$ gap of the $L_x \rightarrow \infty$ system. The vertical (red) line in each inset shows the correspondence with the energy sweep of its panel.

energy E is determined as

$$G(E) = \frac{e^2}{h}[T_N(E) + R_A(E)], \quad (2)$$

where T_N is the normal (electron-electron) transmission probability and R_A is the Andreev (electron-hole) reflection probability. The superconductor is assumed grounded and the applied bias symmetrical since otherwise currents may emerge from the superconductor and flow to the leads [9,30,31].

The resolution method describes both longitudinal and transverse evanescent behavior, an essential point since we are interested in the dependence with both L_x and L_y . Including large-enough sets of $N_k \approx 100$ complex- k waves for each region describes longitudinal evanescent behavior while a uniform y spatial grid with $N_y \approx 100$ points is required to describe the transverse behavior. In addition, a minimal grid of only $N_x = 5$ points for each interface is required for the matching. The computational cost is small and, quite importantly, it is independent of L_x , which is again essential for the study of the L_x dependence up to large values.

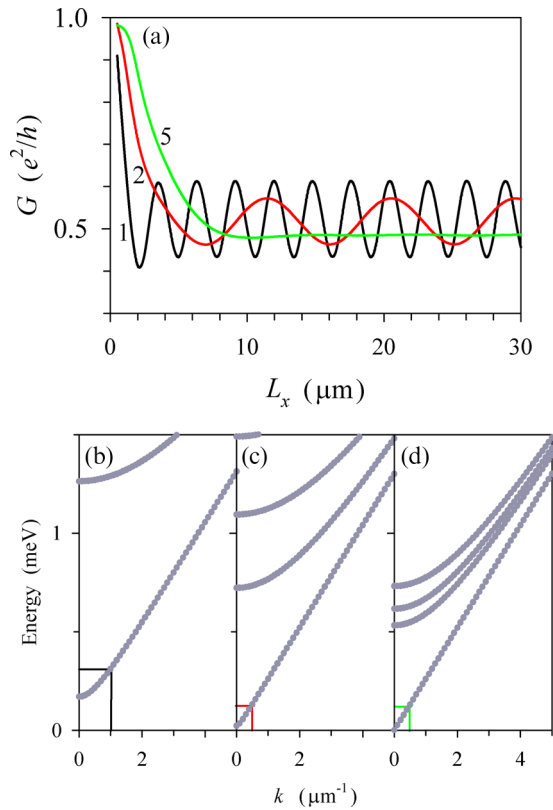


FIG. 2. (a) L_x dependence of the conductance for different values of the width L_y , as indicated by the number close to each line (in microns). The results correspond to those in Fig. 1 for selected values of the energy: 0.3 meV ($L_y = 1 \mu\text{m}$), 0.09 meV ($L_y = 2 \mu\text{m}$), 0.1 meV ($L_y = 5 \mu\text{m}$). (b)–(d) Energy bands for the corresponding values of L_y . The energy and wave number are indicated in each panel with the same line color of (a).

Results. Figure 1 shows a characteristic evolution of bias-dependent conductance $G(E)$ as the strip width L_y increases: $1 \mu\text{m}$ [Fig. 1(a)], $2 \mu\text{m}$ [Fig. 1(b)], and $5 \mu\text{m}$ [Fig. 1(c)]. As expected, the wide strip shows a low-energy flat conductance of $0.5e^2/h$ that, when increasing E , evolves into a complicated variation due to the successive activation of higher-energy modes of the strip. The value of δ , the $k = 0$ gap energy, is shown for each mode as a function of Δ_Z in the corresponding insets of Fig. 1. In the narrower strips of Figs. 1(a) and 1(b) the flat $0.5e^2/h$ plateau transforms into a clear oscillating pattern, with a larger amplitude at the onset and gradually damping with increasing energies. This pattern is clearly enhanced in the smaller L_y strip [Fig. 1(a)]. A sudden change of this pattern occurs when a second chiral mode is activated, setting in a larger amplitude envelope oscillation between zero and one conductance quantum in Figs. 1(a) and 1(b).

The oscillating conductance in the regime of a single chiral mode of a narrow strip is the main result of this Rapid Communication. It is a sizable effect, easily reaching 40%–50% conductance variations for energies near the activation onset of Fig. 1(a). Next, we study the role of the longitudinal distance L_x on the oscillation. Figure 2 shows $G(L_x)$ corresponding to selected transverse widths and energies of Fig. 1. This figure provides a quantitative measure of the contribution

of longitudinal evanescent modes to the conductance. In all cases G initially decreases from a value close to one, reaching a sustained regime after a critical value of L_x is exceeded. In the narrower strips the asymptotic- L_x regime again reproduces the oscillating pattern mentioned above.

The separation between successive conductance maxima (minima) of the sustained oscillations of Fig. 2(a) can be related to the speed of the chiral Majorana mode. This connection is clear from a direct comparison between the computed real band structure of the propagating modes shown in Figs. 2(b)–2(d). The approximate Majorana mode is represented by the lowest band with an almost linear dependence on wave number, $E \approx c\hbar k$, with $c \approx 0.26 \text{ meV } \mu\text{m}/\hbar$. Assuming a conductance maximum requires an integer number of half wavelengths fit in distance L_x , we infer $c = \Delta L_x E / \pi$, where ΔL_x is the separation of two successive maxima. This reproduces $c \approx 0.26 \text{ meV } \mu\text{m}/\hbar$ for the $L_y = 1$ and $2 \mu\text{m}$ results of Fig. 2(a), respectively.

As explicitly shown above, measuring $G(L_x)$ allows an electrical determination of the mode speed. The same conclusion is obtained inferring c from the separation energy ΔE between two successive maxima of the oscillation pattern $G(E)$ of Figs. 1(a) and 1(b). In this case, however, the oscillation is not sustained for arbitrary large values, but one has to choose E in the proper interval corresponding to the propagation of a single chiral mode. There is a clear analogy between our model system and a photon interferometer, similarly to other condensed matter systems such as Aharonov-Bohm rings, with the genuine difference that in a strip the interference of chiral modes is governed by the interplay between strip dimensions L_x, L_y and the mechanism of Andreev backscattering. Incidentally, in units of the photon speed in vacuum, the chiral mode speed of Fig. 2 is $\approx 1.3 \times 10^{-3}$.

We now elucidate from our calculations the physical mechanism behind the enhanced conductance when condition $L_x = n\lambda/2$ is fulfilled, with n an integer and λ the wavelength of the chiral mode between the two interfaces. Figure 3 shows that the conductance oscillation basically reflects the behavior of the Andreev reflection probability R_A , and the normal transmission T_N is also oscillating but with a weaker amplitude and a reduced wavelength. The contour plots displayed in Figs. 3(b)–3(e) show the distribution of quasiparticle probability density corresponding to an incidence from the upper left chiral mode. As expected, in the superconducting piece of the strip, transmission proceeds predominantly attached to the upper edge. A zoom of the lower edge reveals that in Fig. 3(c) two full intervals between density maxima fit in L_x , counting backwards from the lower right maximum, while in Fig. 3(e) two and a half intervals can fit in. As the distance between density maxima is $\lambda/2$, this is the interference of the backscattered chiral mode from the right interface that can thus enhance or decrease the global Andreev reflection from the left interface.

Edge chiral Majorana modes are robust against backscattering induced by local disorder, in a similar way to the quantum Hall effect. We have checked (see Supplemental Material [21]) that the conductance oscillations of this work are indeed robust with the presence of local fluctuations $\delta m_0(x, y)$ in a portion of the strip modeling bulk disorder as well as deviations from perfect straight edges. As a final result,

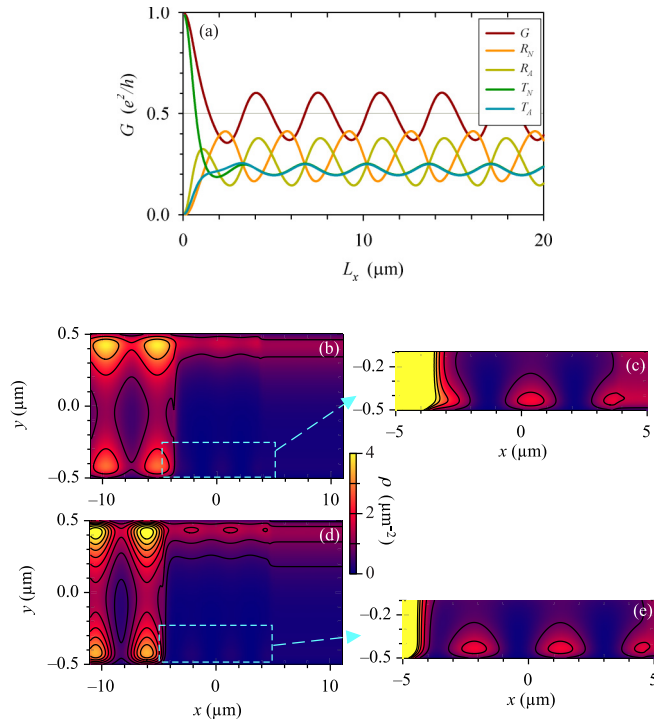


FIG. 3. (a) Evolution with L_x of normal and Andreev reflections and transmissions for a strip of $L_y = 1 \mu\text{m}$ and energy $E = 0.25 \text{ meV}$. (b)–(e) Spatial distribution of probability density, in μm^{-2} , corresponding to the conductance (b) maximum at $L_x = 7.5 \mu\text{m}$ and (d) minimum at $L_x = 9.3 \mu\text{m}$. (c) and (e) show the densities in a $10\times$ -zoomed scale for the highlighted regions.

we have considered the presence of side *material* barriers in the longitudinal direction by assuming $m_0 \equiv m_{0b} = 2 \text{ meV}$ in regions of length L_b to the left and right of the superconductor central island of the strip. As with the usual potential barriers, the transparency of those side regions can be tuned by changing m_{0b} and/or L_b . The presence of side barriers tends to decouple leads and the central island, leading to a more clear manifestation of the interferometer character discussed above. Figure 4 shows how the oscillating pattern of $G(E)$ evolves to a sequence of spikes as the barriers

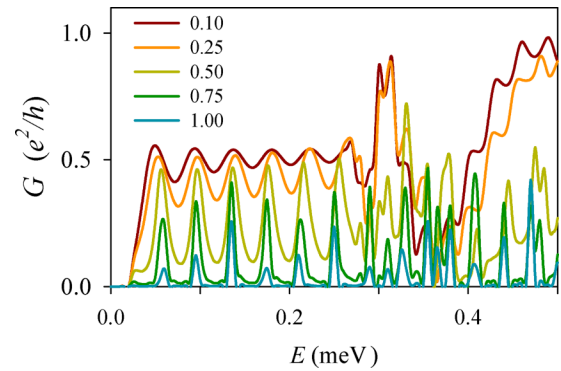


FIG. 4. $G(E)$ in the presence of barriers to the left and right of the strip superconductor region. The different curves correspond to varying barrier lengths L_b , as indicated in microns. We take $m_{0b} = 2 \text{ meV}$ in the barrier sections of the strip. Other parameters as in Fig. 1(b).

become less and less transparent, each spike signaling the condition of resonant backscattering of the chiral Majorana mode. Thus, the configuration with side barriers suggests a device operation with a clearer difference between its on and off states.

Conclusion. In summary, our calculations suggest that a quantum anomalous Hall thin strip with a central superconductor section could display conductance oscillations when the strip transverse size L_y is in the micrometer range and the system is in a fully quantum coherent regime. As a function of the superconductor region length L_x , the oscillations are sustained up to arbitrary large values. We conclude that a quantum mesoscopic strip behaves as an interferometer that allows measuring the speed of the chiral Majorana mode. The physical mechanism is the enhanced Andreev reflection due to resonant backscattering of the chiral mode from the second to the first interface. The presence of side barriers magnifies the interferometer effect by yielding conductance spikes.

This work was funded by MINEICO (Spain), Grant No. MAT2017-82639.

- [1] C. Nayak, S. H. Simon, A. Stern, M. Freedman, and S. Das Sarma, *Rev. Mod. Phys.* **80**, 1083 (2008).
- [2] V. Mourik, K. Zuo, S. M. Frolov, S. R. Plissard, E. P. A. M. Bakkers, and L. P. Kouwenhoven, *Science* **336**, 1003 (2012).
- [3] Ö. Gül, H. Zhang, J. D. S. Bommer, M. W. A. de Moor, D. Car, S. R. Plissard, E. P. A. M. Bakkers, A. Geresdi, K. Watanabe, T. Taniguchi, and L. P. Kouwenhoven, *Nat. Nanotechnol.* **13**, 192 (2018).
- [4] H. Zhang, C.-X. Liu, S. Gazibegovic, D. Xu, J. A. Logan, G. Wang, N. van Loo, J. D. S. Bommer, M. W. A. de Moor, D. Car, R. L. M. Op het Veld, P. J. van Veldhoven, S. Koelling, M. A. Verheijen, M. Pendharkar, D. J. Pennachio, B. Shojaei, J. S. Lee, C. J. Palmström, E. P. A. M. Bakkers *et al.*, *Nature (London)* **556**, 74 (2018).
- [5] R. Aguado, *Riv. Nuovo Cimento* **40**, 523 (2017).
- [6] R. M. Lutchyn, E. P. A. M. Bakkers, L. P. Kouwenhoven, P. Krogstrup, C. M. Marcus, and Y. Oreg, *Nat. Rev. Mater.* **3**, 52 (2018).
- [7] Q. L. He, L. Pan, A. L. Stern, E. C. Burks, X. Che, G. Yin, J. Wang, B. Lian, Q. Zhou, E. S. Choi, K. Murata, X. Kou, Z. Chen, T. Nie, Q. Shao, Y. Fan, S.-C. Zhang, K. Liu, J. Xia, and K. L. Wang, *Science* **357**, 294 (2017).
- [8] X.-L. Qi, T. L. Hughes, and S.-C. Zhang, *Phys. Rev. B* **82**, 184516 (2010).
- [9] S. B. Chung, X.-L. Qi, J. Maciejko, and S.-C. Zhang, *Phys. Rev. B* **83**, 100512 (2011).
- [10] J. Wang, B. Lian, H. Zhang, and S.-C. Zhang, *Phys. Rev. Lett.* **111**, 086803 (2013).

- [11] J. Wang, B. Lian, and S.-C. Zhang, *Phys. Rev. B* **89**, 085106 (2014).
- [12] J. Wang, Q. Zhou, B. Lian, and S.-C. Zhang, *Phys. Rev. B* **92**, 064520 (2015).
- [13] B. Lian, J. Wang, and S.-C. Zhang, *Phys. Rev. B* **93**, 161401 (2016).
- [14] Y.-T. Zhang, Z. Hou, X. C. Xie, and Q.-F. Sun, *Phys. Rev. B* **95**, 245433 (2017).
- [15] Y.-F. Zhou, Z. Hou, Y.-T. Zhang, and Q.-F. Sun, *Phys. Rev. B* **97**, 115452 (2018).
- [16] R. W. Reinthaler, P. Recher, and E. M. Hankiewicz, *Phys. Rev. Lett.* **110**, 226802 (2013).
- [17] A. R. Akhmerov, J. Nilsson, and C. W. J. Beenakker, *Phys. Rev. Lett.* **102**, 216404 (2009).
- [18] L. Fu and C. L. Kane, *Phys. Rev. Lett.* **102**, 216403 (2009).
- [19] H. S. Røising and S. H. Simon, *Phys. Rev. B* **97**, 115424 (2018).
- [20] S. Das Sarma, J. D. Sau, and T. D. Stanescu, *Phys. Rev. B* **86**, 220506 (2012).
- [21] See Supplemental Material at <http://link.aps.org/supplemental/10.1103/PhysRevB.98.121407> for details on our method to solve the scattering equations and for additional results not shown in the main text.
- [22] L. Serra, *Phys. Rev. B* **87**, 075440 (2013).
- [23] J. Osca and L. Serra, *Phys. Rev. B* **91**, 235417 (2015).
- [24] J. Osca and L. Serra, *Eur. Phys. J. B* **90**, 28 (2017).
- [25] J. Osca and L. Serra, *Phys. Status Solidi B* **254**, 1700135 (2017).
- [26] J. Osca and L. Serra, *Beilstein J. Nanotechnol.* **9**, 1194 (2018).
- [27] F. Tisseur and K. Meerbergen, *SIAM Rev.* **43**, 235 (2001).
- [28] R. B. Lehoucq, D. C. Sorensen, and C. Yang, *ARPACK Users Guide: Solution of Large-Scale Eigenvalue Problems with Implicitly Restarted Arnoldi Methods* (SIAM, Philadelphia, 1998).
- [29] C. S. Lent and D. J. Kirkner, *J. Appl. Phys.* **67**, 6353 (1990).
- [30] C. J. Lambert, V. C. Hui, and S. J. Robinson, *J. Phys.: Condens. Matter* **5**, 4187 (1993).
- [31] J. S. Lim, R. López, and L. Serra, *New J. Phys.* **14**, 083020 (2012).